ARTICLE

Fibronectin Adsorption, Cell Adhesion, and Proliferation on Nanostructured Tantalum Surfaces

A. Dolatshahi-Pirouz,[†,‡] T. Jensen,[†,§] David Christian Kraft,[⊥] Morten Foss,[†,*] Peter Kingshott,[†] John Lundsgaard Hansen,[‡] Arne Nylandsted Larsen,[‡] Jacques Chevallier,[‡] and Flemming Besenbacher[†,‡]

[†]Interdisciplinary Nanoscience Center (iNANO), and [‡]Department of Physics and Astronomy, Aarhus University, Aarhus, Denmark, [§]Orthopaedic Research Laboratory, Aarhus University Hospital, Aarhus, Denmark, and [⊥]Department of Orthodontics, School of Dentistry, Aarhus University, Aarhus, Denmark

ABSTRACT The interaction between dental pulp derived mesenchymal stem cells (DP-MSCs) and three different tantalum nanotopographies with and without a fibronectin coating is examined: sputter-coated tantalum surfaces with low surface roughness <0.2 nm, hut-nanostructured surfaces with a height of 2.9 ± 0.6 nm and a width of 35 ± 8 nm, and dome structures with a height of 13 ± 2 nm and a width of 52 ± 14 nm. Using ellipsometry, the adsorption and the availability of fibronectin cell-binding domains on the tantalum surfaces were examined, as well as cellular attachment, proliferation, and vinculin focal adhesion spot assembly on the respective surfaces. The results showed the highest fibronectin mass uptake on the hut structures, with a slightly higher availability of cell-binding domains and the most pronounced formation of vinculin focal adhesion spots as compared to the other surfaces. The proliferation of DP-MSCs was found to be significantly higher on dome and hut surfaces coated with fibronectin compared to the uncoated flat tantalum surfaces. Consequently, the results presented in this study indicate that fibronectin-coated nanotopographies with a vertical dimension of less than 5 nm influence cell adhesion. This rather interesting behavior is argued to originate from the more available fibronectin cell-binding domains observed on the hut structures.

KEYWORDS: nanotopography · tantalum · fibronectin · mesenchymal stem cells · cell adhesion · tissue engineering · protein adsorption

Biomaterials play an important role in bioengineering applications such as regenerative medicine, tissue engineering, biosensing, and in orthopedics.[1] For orthopedic implants, an early bone formation and strong binding between bone and implant are important for the long-term success of the implant.[1] The ability of osteogenic cells to adhere, proliferate, and differentiate on the biomaterial surface is crucial for the formation of new bone tissue and the subsequent osseointegration of the implant.

Since bone is a hierarchically composed material,[2] osteogenic cells encounter topographical features with different sizes in their natural environment, from macrofeatures such as the bone structure to micro- and nanoscale features such as the shape of cells, fiber networks, mineral crystallites,[2,3] and interconnecting pores.[2,4−6] Therefore, the design of topographical implant surfaces holds promise to be part of the fabrication of the next generation of superior medical implants.[2,4−6] The majority of cell studies performed on topographically altered surfaces have mainly focused on lithographically produced micrometer scale (>1000 nm) and submicrometer scale structures (100−1000 nm).[7−22] The results indicate that the surface topography may influence cell adhesion,[8,13,14,18] cell morphology,[9,10,16,22] mineralization, and gene expression.[15,17,21] Recently, several reports have likewise shown that nanoscale surface features (<100 nm) can affect focal contact assembly on a surface,[9,23−26] cell adhesion,[27−29] and proliferation.[30] However, only a few studies exist in which the cellular response on surface topographies with vertical dimensions ≤10 nm is investigated.[31,32] For example, it has been shown that osteoblast cells are sensitive to topographic features with a surface feature height as small as 5 nm.[32] Since fibronectin (Fn) is able to specifically interact with cells through a arginine-glycine-aspartic acid (RGD) sequence, the performance of biomaterials can also be vastly improved by a Fn coating.[33−40] Accordingly, one might anticipate that Fn-coated nanostructured materials could further enhance the positive effects that accompany nanostructured surfaces. Despite the numerous studies that explore the interaction between cells and Fn-coated biomaterials,[33−40] we only know of one study that has examined cellular responses to materials with a well-defined nanotopography coated with Fn.[41]

Motivated by the few reported studies on cell interactions on Fn-coated nanostructured materials and surface structures with dimensions below 10 nm, we decided to examine the interaction between dental pulp

*Address correspondence to foss@inano.au.dk.

Received for review December 8, 2009 and accepted April 20, 2010.

Published online May 5, 2010.
10.1021/nn9017872

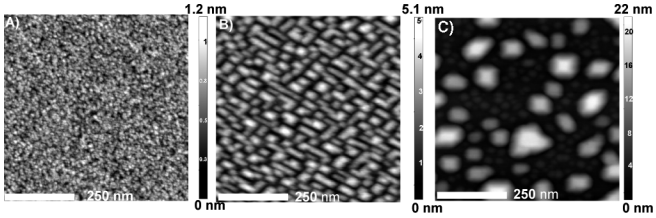

Figure 1. Representative Atomic Force Microscopy (AFM) images of the tantalum surfaces employed in the cell experiments. The *z*-range value appears as the largest number in the gray scale bars. (a) Tantalum surface used as the flat reference [F], (B) huts [H], and (C) domes [D].

derived mesenchymal stem cells (DP-MSCs) and Fn-coated surface features with a vertical height below 5 nm. Nanostructured Ge−Si surfaces with geodesic hemispheres typically denoted as domes in the literature[42] with side plane slopes at 25.2° ({113} facet) and 26.6° ({102} facet) or small triangular prisms with an average height below 5 nm and a slope at 10.9° ({105 facet}), referred to as huts,[43] were fabricated by exploring the molecular beam epitaxy (MBE) deposition technique as has been done in previous studies.[42−45] The respective surfaces were afterward coated with a thin tantalum layer, a material often used in orthopedic implants.[46] The Fn adsorption and the availability of the cell-binding domains on the respective nanostructured tantalum surfaces were determined by ellipsometry. DP-MSCs were subsequently cultured on substrates with and without a Fn coating to evaluate the effect of Fn-coated nanoscale surface features on the proliferation, cytoskeletal organization, and the assembly of vinculin focal adhesion spots in the cells.

RESULTS

Characterization of the Tantalum Surfaces. The AFM images of the tantalum reference surface are presented in Figure 1A along with the nanostructured tantalum surfaces denoted as huts (Figure 1B) and domes (Figure 1C). The hut surface consisted of very delicate surface features with dimensions of 2.9 ± 0.6 nm in height, 35 ± 8 nm in width, and 84 ± 20 nm in length, while the domes were more variable in size with dimensions of 13 ± 2 nm in height, 52 ± 14 nm in width, and 121 ± 37 nm in length. On the flat reference, no distinct structures were recognized (Figure 1A). The root-mean square (rms) roughness values[47] were quantified as 0.151 ± 0.012, 0.80 ± 0.05, and 4.45 ± 0.06 nm on flat, hut and dome surfaces respectively (Table 1). The roughness factor values (1.002−1.007) show that the surface area increase compared to that of an atomically flat surface was quite small on the respective surfaces and therefore would not result in significantly more available surface adsorption sites when the surfaces are compared to one another. Even though the values presented in Table 1 are in the same range as the ones determined by Riedel *et al.*,[29] they might be underestimated due to both the finite resolution of the AFM instrument and tip convolution effects.[30] In addition to the morphology analysis by AFM, we also employed XPS to characterize the respective surface chemistries (Table 2). Besides the presence of tantalum and oxygen, traces of carbon were also observed on all samples. The presence of carbon originates from surface contamination caused by exposure to air after the sputtering step. Hydrocarbon is unavoidable and will always be present on these types of surfaces. Within the uncertainties, we did not find any differences in the chemical compositions of the respective surfaces (Table 2). Moreover, the O/Ta ratio was similar on the respective surfaces and ranged from 2.30 to 2.46, which is close to the stoichiometry of Ta_2O_5. Since all the surfaces were hydrophilic as well after 25−30 min UV treatment, this means that any observed differences in both protein adsorption and cell attachment/proliferation on the respective surfaces would, in fact, be due to different surface morphologies.

Fibronectin Adsorption Results. Fibronectin (Fn) adsorption on the flat reference, hut, and dome surfaces was followed in real time by ellipsometry.[49−51] Each adsorption experiment was stopped after 60 min, and the obtained saturated surface mass densities ($\Gamma_{Ellipsometry}$) from the respective surfaces are listed in Table 3. On the hut surfaces, the Fn adsorption was 378 ± 10 ng/cm^2, significantly higher than Fn surface mass densities determined on either the dome or the flat reference surface. Since the roughness factor was almost the same on the hut and flat reference surface, the enhanced surface mass uptake observed on the hut surface is caused by nontrivial adsorption effects beyond a simple surface area increase.[29,30,52] No surface mass density difference was observed between dome and flat reference surface (the Fn surface mass density attained the value 294 ± 19 ng/cm^2 on the flat reference and 295 ± 17 ng/

TABLE 1. Different Surface Parameters Found with Atomic Force Microscopy[a]

surface	height [nm]	width [nm]	length [nm]	rms value [nm]	roughness factor (*R*)
flat	*b*	*b*	*b*	0.151 ± 0.012	1.002 ± 0.002
hut	2.9 ± 0.6	35 ± 8	84 ± 20	0.80 ± 0.05	1.007 ± 0.004
dome	13 ± 3	52 ± 14	121 ± 37	4.45 ± 0.06	1.030 ± 0.004

[a]The roughness factor (*R*) is defined as the surface area compared to a completely flat surface, $R = A_{surface}/A_{flat\ surface}$. [b]Not applicable.

TABLE 2. XPS Surface Analysis of the Respective Surfaces (Values Are Shown as Mean ± Standard Error of the Mean)

surface	Ta_{4d}	C_{1s}	O_{1s}	O_{1s}/Ta_{4d}
flat	25.8 ± 0.2	15.1 ± 1.5	59.3 ± 1.2	2.30 ± 0.05
hut	25.0 ± 1.1	13.6 ± 0.6	61.4 ± 1.0	2.46 ± 0.12
dome	25.5 ± 0.1	14.3 ± 0.6	60.2 ± 0.6	2.36 ± 0.03

TABLE 3. Fibronectin Surface Mass Density ($\Gamma_{ellipsometry}$) and the Number of Antibodies Per Protein Obtained by Ellipsometry (Values Are Shown as Mean ± Standard Error of the Mean)

surface	$\Gamma_{ellipsometry}$ [ng/cm^2]	antibodies per protein
flat	294 ± 19	0.64 ± 0.03
hut	378 ± 10[a]	0.793 ± 0.012[b]
dome	295 ± 17	0.73 ± 0.04

[a]Represents statistical difference of $p < 0.01$ compared to the reference tantalum (F) and dome surface (D). [b]Represents statistical difference of $p < 0.01$compared to the reference tantalum surface (F).

cm^2 on the dome surface). The availability of the cell-binding domains on Fn was assayed with ellipsometry by using a special monoclonal antibody[48] which recognizes the cell-binding domains on Fn (Table 3). The individual Fn proteins on the hut surfaces were found to bind 0.79 ± 0.01 antibodies per Fn molecule, which was significantly higher than on the flat reference surface (0.64 ± 0.03). On the other hand, 0.73 ± 0.04 antibodies bound to the Fn-coated dome surface, which is not statistically different compared to the result obtained on the flat reference surface and the hut surface. The differences found in Table 3 among the different surface types can solely be attributed to morphological differences given that the surface chemistry was similar on the flat, hut, and dome surfaces. The amount of nonspecific antibody binding on the respective surfaces was also followed with the ellipsometry technique, showing a nonspecific binding, which was less than 5% and significantly lower than the difference between the antibody results on the hut surface and the flat reference surface (19%) and thus not the main reason for these differences.

Even though these nonspecific binding values might be overestimated due to BSA contaminants in the fibronectin solution, this does not change the interpretation of the antibody results because the BSA contaminants would result in an even lower nonspecific binding (<5%).

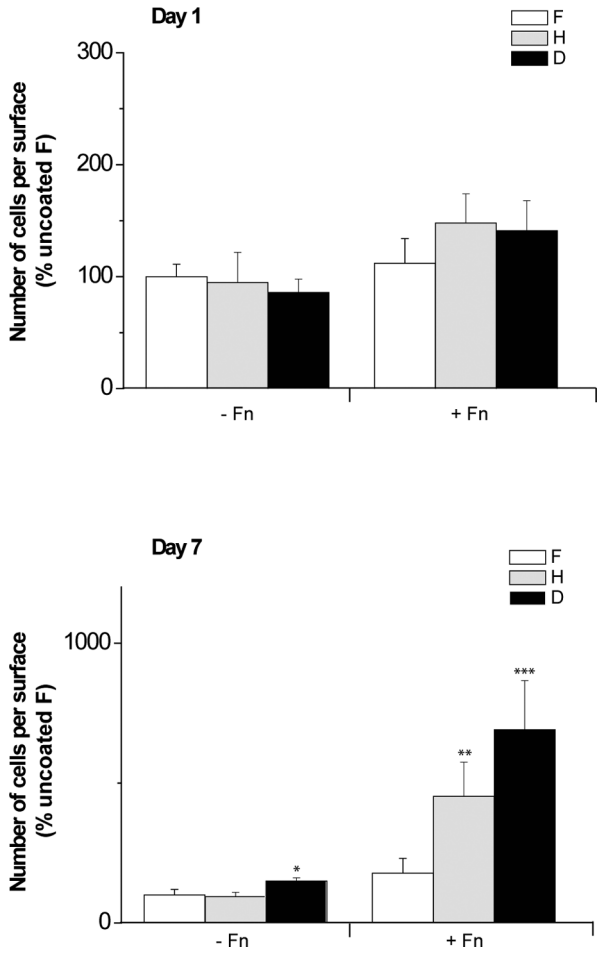

Figure 2. Total number of cells attached to the different surfaces after day 1 and day 7. The number of cells counted per surface has been normalized with respect to the amount of cells that attached to the reference tantalum surface without fibronectin (−Fn). Values are shown as mean ± standard error of the mean from 5 data points ($n = 5$). At day 1, the differences in the number of cells on the different samples were not statistically different. The symbol * represents statistical difference of $p < 0.05$ compared to the uncoated (−Fn) surface with huts (H) after day 7; ** represents statistical difference of $p < 0.05$ compared to the uncoated (−Fn) reference surface (F) and the uncoated (−Fn) surface with huts (H) after day 7; * represents statistical difference of $p < 0.05$ compared to the uncoated (−Fn) reference surface (F), the uncoated (−Fn) surface with huts (H), the uncoated (−Fn) surface with domes (D), and the coated (+Fn) reference surface (F) after day 7.**

Cell Proliferation and Attachment. Attachment and proliferation of DP-MSCs as quantified after 1 day and 7 days on the flat reference, hut, and dome surfaces with or without an initial Fn coating are depicted in Figure 2. No significant differences in attachment were observed between the different surfaces after 1 day, and most importantly, it was found that the Fn coating itself did not have any effect on the cell attachment.

For the uncoated surfaces after a period of 7 days, a statistically different number of cells per surface were only observed between the uncoated dome and hut surface (Figure 2). On the Fn-coated surfaces, a significantly higher proliferation was observed on the hut and dome surfaces as compared to their uncoated counterparts, while no significant difference was observed between the Fn-coated and uncoated flat reference surface. Furthermore, the coated dome surfaces were found to have a significantly higher proliferation as compared to the Fn-coated reference surface as well as all the uncoated ones.

Cytoskeleton Organization and Quantification of Focal Adhesion Points. The cytoskeleton organization on the respective surfaces was investigated with an fluorescence triple staining of the actin (cytoskeleton), vinculin (focal adhesion protein), and cell nucleus (see Figure 3). As is depicted in Figure 3, cells were well-spread with many contracted and well-defined actin stress fibers on all surfaces. Assessment of the formation of focal contacts between the cells and the respective surfaces was performed by examining the

assembly of vinculin proteins into dot-shaped structures in the respective cells by using ImageJ (Figure 3). By comparing the images in Figure 3 qualitatively with one another, it is evident that more vinculin focal contacts are formed on the Fn-coated flat reference and hut surfaces as compared to their uncoated counterparts, while no obvious differences were observed between the coated and uncoated dome surfaces. Moreover, in general, a higher number of vinculin spots were observed on the coated hut surface as compared to the coated flat reference and dome surfaces (Figure 3). From a more detailed investigation of the cell border, a significantly higher number of filopodia extensions were seen on all of the Fn-coated surfaces as compared to the uncoated ones (Figure 4). By comparing the number of filipodia per cell among the coated surfaces, no significant difference was observed between flat and dome surfaces, while a significant higher number of filopodia per cell were observed on the hut surface as compared to flat and dome surfaces.

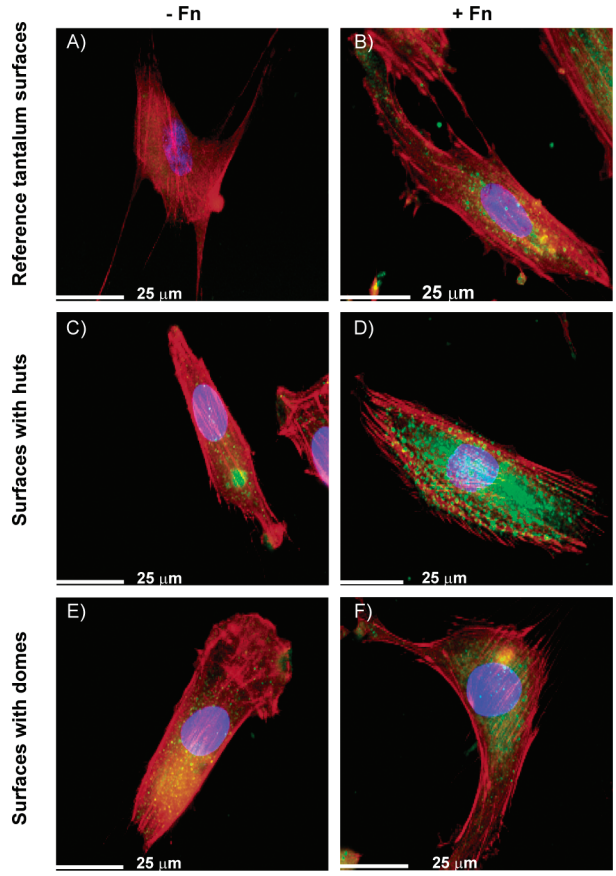

Figure 3. Actin (red), vinculin (green), and cell nucleus (blue) fluorescence images of the cells after 24 h of culture. (A) On the reference uncoated (−Fn) tantalum surface, only few vinculin focal adhesion spots were found, in general, while the actin cytoskeleton was seen to be well-organized with many stress fibers. (B) On the fibronectin-coated (+Fn) reference, tantalum surface focal adhesion spots were clearly seen together with well-developed actin stress fibers. (C) Despite of a well-organized actin cytoskeleton on the uncoated (−Fn) surface with huts, only few and very faint vinculin focal adhesion spots were seen as compared to (D) the fibronectin-coated (+Fn) surface with huts. (E,F) Vinculin focal adhesion spots together with a well-developed actin cytoskeleton were observed on both the uncoated (−Fn) and the coated (+Fn) surface with domes; however, there were no differences among these two surfaces in the assembly of vinculin into focal spots.

DISCUSSION

Several studies have shown that nanostructured surfaces are able to influence cell behavior.[4−6] However, more detailed studies of the cellular responses on nanostructured surfaces with dimensions below 10 nm remain to be further elucidated as nanofeatures in this range are postulated to play an important role in directing the process of bone formation and regeneration.[2,4] In the present study, we have shown that osteogenic cells interact stronger with fibronectin (Fn)-coated nanostructured hut surfaces with vertical dimensions below 5 nm as compared to a flat reference surface.

The formation of the Fn coatings on the respective surfaces was followed with ellipsometry (see Table 3), showing a significantly higher Fn surface mass density on the hut surface as compared to the flat reference and dome surface, while no differences were observed between the flat and dome surfaces.

Accordingly, the ellipsometry results indicate that the conformation/orientation of the individual Fn molecules is different on the hut surface as compared to the dome and flat reference surfaces. The higher Fn surface mass density found on the hut surface was also accompanied by more antibodies specifically binding to the cell-binding domains on Fn as compared to the other surface types. Since it has been shown in several recent reports that the surface topography can change the conformation of proteins in a different way as compared to a flat reference surface,[29,30,41,53,54] it is reasonable to assume that the Fn molecules bind in a different conformation/orientation on the hut surface with more available cell-binding domains. This type of reasoning is supported by a recent study,[29] where germanium nanopyramids acted as preferential adsorption sites for proteins such as BSA and bovine γ-globulin (bgg), resulting in both a larger protein surface mass uptake as well as an impaired bgg functionality as compared to the flat reference surface. However, the increased protein adsorption was more pronounced in ref 29 compared to what we observe in this study for Fn, with a nearly 2−3-fold increased adsorption on the nanostructured germanium surface.[29]

Other reports have shown that the number of antibodies binding to adsorbed Fn decreases as the surface roughness increases.[41,54] For instance in ref 54, the Fn surface mass uptake increased concurrently with surface roughness and was followed by a decrease in the number of monoclonal antibodies binding to the Fn

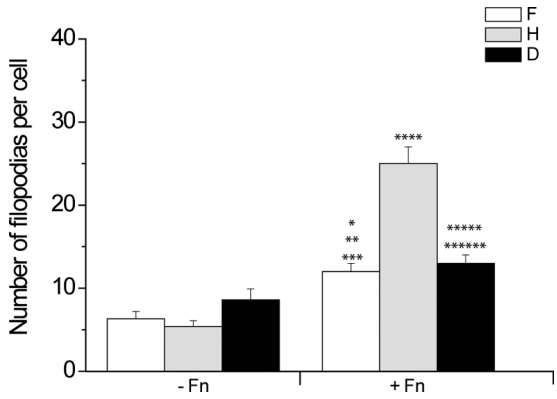

Figure 4. Mean number of filopodia per cell on the different surfaces after the surfaces were seeded with cells for 1 day. Values are shown as mean ± standard error of the mean from 30 data points ($n = 30$). The symbol * represents statistical difference of $p < 0.0005$ compared to the uncoated (−Fn) reference tantalum surface (F); ** represents statistical difference of $p < 0.05$ compared to the uncoated (−Fn) surface with domes (D); * represents statistical difference of $p < 0.0001$ compared to the uncoated (−Fn) surface with huts (H); **** represents statistical difference of $p < 0.0001$ compared to the coated (+Fn) reference tantalum surface (F), the coated (+Fn) surface with domes (D), as well as all the uncoated (−Fn) surfaces; ***** represents statistical difference of $p < 0.0001$ compared to the uncoated (−Fn) reference tantalum surface (F) and the uncoated (−Fn) surface with huts (H); ****** represents statistical difference of $p < 0.001$ compared to the uncoated (−Fn) surface with domes (D).**

proteins opposite to what is observed from the ellipsometry results shown in Table 3.

To examine whether the higher cell-binding domain availability on the Fn molecules on the hut surface is reflected in cell surface interactions, cell proliferation/attachment studies were carried out. The proliferation/attachment assays showed that the cells were more proliferative on the Fn-coated hut surface as compared to the Fn-coated flat reference surface. This is in accordance with a more active Fn coating on the hut surface since Fn through its two cell-binding domains can direct intracellular signaling events such as mineralization, cell proliferation, attachment, and spreading.[33−40] A recent study[41] also revealed a correlation between Fn adsorption on nanostructured surfaces and the subsequent proliferation of cells. Here[41] it was shown that the individual Fn proteins were less active on nanostructured silica surfaces and able to inhibit human endothelial cell proliferation.

Turning to the dome nanostructured surface, a significant difference between the uncoated and coated dome and flat reference surfaces is likewise observed despite a similar Fn coating prior to the cell seeding on these surfaces. It is therefore more likely that a synergistic effect between the surface topography on the dome surfaces and the Fn coating is responsible for the cell proliferation behavior observed on the dome surface, or alternatively, the cells remodel the Fn coating shortly after attaching to the dome surface, leading to more available RGD sequences for cell-guiding purposes.

The proliferation studies were followed up by an investigation of the cell cytoskeleton and assembly of vinculin proteins into focal adhesion spots because the cytoskeleton organization and the formation of focal adhesion contacts is the starting point of a chain of signaling events that could lead to cell proliferation, differentiation, motility, and, in the end, tissue healing.[55−60] These signaling events are initiated by the activation of an important G-protein, Rho, which leads to actin contraction resulting in integrin clustering and the formation of vinculin adhesion spots.[55,56,58]

The number of vinculin focal adhesion spots was largest in the cells attached on the Fn-coated hut surface, and by examining the images in Figure 3 qualitatively, a more intense fluorescence intensity from the individual spots is seen, as well. The results indicate that the integrin clustering was more pronounced on the Fn-coated hut surface as compared to the Fn-coated flat reference surface, in accordance with the larger proliferation observed on the coated hut surface. However, these results are somewhat puzzling since they do not correspond well with the even higher cell proliferation observed on the dome surface.

The fluorescence images also showed that the number of filopodia per cell increase on all surfaces after the surfaces are coated with Fn, where the highest number of filopodia per cell was found on the Fn-coated hut surface. Gustafson and co-workers were the first to discover filopodia in cells, and since then, filopodia[61] have been widely recognized as one of the main sensory kits in cells. Filopodia have been associated with both chemical and topographical sensing of heterogeneous surfaces.[22,23,31]

For instance, in refs 22 and 23, Dalby *et al.* noticed that fibroblast cells are able to sense nanocolumns (100 nm diameter, 160 nm high)[22] as well as 13 nm high polymer demixed islands.[23] In addition, it has also been shown that fibroblast filopodia are able to sense and interact with 10 nm high surface nanofeatures, which to our knowledge is the smallest dimension that has been registered to affect cell sensing on a surface so far.[31] We, therefore, tentatively suggest that a similar topographical sensing might occur on the Fn-coated hut surface compared to the coated flat reference and dome surface, which is an interesting observation since the hut surface consist of very delicate nanostructures with a surface feature height of only 2.9 ± 0.6 nm.

CONCLUSION

We have shown that nanostructured surfaces with a root mean square (rms) roughness value less than 1 nm and surface nanostructures with an aver-

age height <5 nm are able to influence the adsorption of Fn and direct cell surface interactions such as cell proliferation, focal contact assembly, and filopodia expression. To our best knowledge, a rms value of 1.05 ± 0.21 nm and nanostructures with a surface feature height of approximately 5 nm are the smallest surface topographical parameters that have been shown to influence cell/surface interactions thus far.[32] In summary, the results presented here illustrate the importance of a detailed surface characterization at the nanoscale since surface nanostructures with vertical dimensions of a few nanometers as those present on the hut surface may have a significant influence on cellular behavior when coated with Fn, a cell anchoring protein which is present in the majority of cell culture mediums.

METHODS

Proteins and Antibodies. Fibronectin (Fn) extracted from bovine plasma was purchased from Sigma-Aldrich (Broendby, Denmark) and coated on the respective tantalum surfaces by spontaneous adsorption from solution. The cell-binding properties of the individual Fn molecules on the surfaces were determined using a bovine IgG monoclonal anti-fibronectin (BioPorto Diagnostics A/S, Gentofte, Denmark) directed against an epitope located on the two 120 kDa cell-binding domains on fibronectin.[48] Nonspecific binding by IgG monoclonal anti-fibronectin was tested using rabbit IgG polyclonal BSA antibodies (Sigma-Aldrich, Broendby, Denmark). Fn and antibody stocks were stored at −50 °C before being dissolved in a 10 mM Tris buffer to a fibronectin concentration of 100 μg/mL and an antibody concentration at 50 μg/mL with 1 mM CaCl and 100 mM NaCl adjusted with HCl and NaOH to a pH value around 7.4 at 37 °C.

Ellipsometry. Ellipsometry is a well-established technique that has been applied for the past decades to study interfacial protein adsorption.[49,50] It allows *in situ* studies at the solid−liquid interface with a time resolution down to milliseconds and a protein layer thickness resolution around 0.1 nm.[49,50] The measurements were carried out in a static liquid cell with an ELX-02C ellipsometer (DRE GmbH, Ratzeburg, Germany) with a single wavelength, λ = 632.8 nm He−Ne laser at a fixed angle of incidence at 70°. The detection principle behind the ellipsometry technique relies on changes in the polarization of elliptically polarized light reflected from an interface. These changes are monitored by measuring the changes in the ellipsometric angles (Δ, ψ) during adsorption and are subsequently converted to a thickness value for the protein film. From the measured thickness, *d*, it is possible to determine the surface mass density of the adsorbed protein film by de Feijters formula[51]

$$\Gamma_{\text{ellipsometry}} = d\frac{n_{\text{protein}} - n_{\text{buffer}}}{dn/dc} \quad (1)$$

where d*n*/d*c* is the refractive index increment for a given concentration change, n_{protein} and n_{buffer} are the refractive index of the protein and buffer, respectively. The d*n*/d*c* value for proteins is typically 0.18 cm^3/g,[50] and the refractive indexes used for the protein layer and the buffer in this study were $n_{\text{protein}} = 1.46$ and $n_{\text{buffer}} = 1.335$, respectively.[50] Before each measurement, the samples were ozone-cleaned with UV light (Bioforce Nanosciences, Ames, IA) for 30 min.

Cell Culture. Human dental pulp derived mesenchymal stem cells (DP-MSCs) were obtained from an ectopically fully developed third molar tooth of a healthy young adult male age 21 using a protocol approved by The Central Denmark Region Committee on Biomedical Research Ethics. Immediately following surgical removal of the molar tooth, the pulp was retrieved and incubated for 30 min at 37 °C in minimum essential medium (MEM; Gibco, Taastrup, Denmark) containing 3 mg/mL collagenase type I (Worthington Biochem, Freehold, NJ) and 2.4 units/mL Dispase II (Roche Diagnostics, Mannheim, Germany). The DP-MSCs liberated from the pulp were passed through a 100 μm strainer (BD Biosciences, Discovery Labware, Bedford, MA). The obtained DP-MSCs were grown in 75 cm^2 culture flasks (Costar, Cambridge, MA) in MEM supplemented with 10% fetal bovine serum (FBS) (PAA Laboratories, Linz, Austria) and antibiotics (25.000 IU/mL penicillin and 25 mg/mL streptomycin, DuraScan Medical Products AS, Odense, Denmark) at 37 °C. Medium was changed twice per week. Upon reaching approximately 90% confluency, the DP-MSCs were harvested using 0.25% trypsin (MEM; Gibco, Taastrup, Denmark) and 0.1% EDTA (Invitrogen, Taastrup, Denmark) in PBS at pH 7.4. In total, five tantalum surfaces of each surface type were placed in either 1 mL of 100 μg/mL Tris fibronectin solution in order to coat the respective surface with fibronectin or 1 mL of pure Tris buffer at room temperature (uncoated surfaces). After 60 min, the wells were washed in medium containing MEM and supplemented with 10% fetal bovine serum (FBS) (PAA Laboratories, Linz, Austria) and antibiotics (25 000 IU/mL penicillin and 25 mg/mL streptomycin, DuraScan Medical Products AS, Odense, Denmark) to avoid transference of free fibronectin to the incubation wells. The surfaces were placed in 6-well plates (Costar, Cambridge, MA) filled with medium to avoid drying, and the DP-MSCs were seeded at a density of 10 000 per cm^2 surface and allowed to attach for 1 day or proliferate for 7 days. Afterward, cells were counted on each surface by harvesting cells from the culture surface by trypsinations and hereafter resuspending the cells in PBS. Cell concentrations were determined with a 100 μm deep Bürker-Türk hemocytometer (BT, Brand, Wertheim, Germany). Counts were performed using a light microscope (Olympus, Ballerup, Denmark) set at 200× magnification and phase contrast magnification and phase contrast. Cell count data were calculated as cells per surface cm^2.

Fluorescence Staining. Fluorescence staining of the actin (cytoskeleton), vinculin (focal adhesion protein), and cell nucleus was performed with a triple staining kit from Chemicon (Chemicon International, Temecula, CA). Throughout the staining procedure, PBS (pH 7.4 at 25 °C) (Sigma-Aldrich, Broendby, Denmark) was used as washing buffer. Cells were washed twice, permeabilized with 0.1% Triton X-100 (Sigma-Aldrich, Broendby, DK), and washed twice again with PBS buffer. The cells were then incubated for 30 min at room temperature with a 1% bovine serum albumin blocking agent and washed twice with PBS buffer. Mouse monoclonal anti-vinculin 1.25 μg/mL was added to the cells and incubated for 60 min at 37 °C and washed three times in PBS. Fluorescein isothiocyanate (FITC)-conjugated goat anti-mouse IgG (10 μg/mL) from Chemicon (Chemicon International, Temecula, CA) and tetramethyl rhodamine isothiocyanate (TRITC)-conjugated phalloidin (37.5 ng/mL) were added to the surfaces and incubated for 60 min at room temperature. Cells were hereafter washed three times with PBS and finally incubated for 5 min at room temperature with 0.1 μg/mL 4,6-diamidino-2-phenylindole (DAPI) and washed three times. Stained cells were kept in PBS at 4 °C. The fluorescence stained cells were subsequently analyzed with a Leica DM 6000B microscope, and 20−25 pictures at 400× magnification were acquired at random on each surface. Subsequently, the contrast and brightness of the respective images were slightly changed to enhance the sharpness of the individual images using ImageJ (freeware from www.rsbweb.nih.gov). Around 30 cells were selected randomly for the quantification of the number of filipodia. Cells that were clustered together were omitted in the analysis of the filopodia expression in the respective cells. The total number of filopodia per cell was then counted by eye.

Surface Preparation and Characterization. The nanostructured surfaces were produced by Si/Ge molecular beam epitaxy (MBE). In brief, a 4 in. (100) silicon wafer with a resistivity of 1−30 Ω·cm and thickness of 300 μm (Si-Mat, Landsberg, Germany) was

cleaned by annealing cycles (500−825 °C) combined with a 600 Å Si buffer layer to relieve stress that could in the worst case result in lattice dislocations. The Si growth was followed by alternating deposition of Si and Ge in an MBE chamber at a pressure of 3×10^{-10} mbar. This type of alternating growth leads to stress-relieved self-assembly of delicate surface nanoprotrusions, due to the lattice misfit between the Ge and Si layers (Ge lattice constant is 4% larger).[62−64] Previous studies have shown that the surface feature spacing, characteristic widths, and surface feature type (hut, pyramid, and dome), in fact, can be controlled by a series of Si and Ge depositions.[42,43,62−64] For instance, alternating deposition of Si and Ge favors the growth of triangular-shaped hut structures, while deposition of more Ge favors the growth of dome structures.[42,43] In this particular study, the hut structures were grown by deposition of 8 Å Ge followed by 2 Å Si and four steps of (2 Å Ge + 2 Å Si) at 560 °C. The domes were grown by depositing 36 Å Ge (560 °C) followed by 15 Å Si (300 °C). Finally, both the hut and dome surfaces were cooled to 300 °C and an additional thin (20 Å) Si layer was deposited on the surface. The tantalum coating was carried out by depositing a 2 nm chromium wetting layer followed by a 20 nm thick tantalum layer. The flat reference tantalum surfaces were produced by sputter depositing a Si wafer with a 100 nm thick tantalum layer (target from Cerac, WI; purity 99.95%). All of the tantalum sputter depositions were carried out at room temperature with an argon pressure of 2×10^{-3} mbar.

The surface morphology and roughness of the thin films were analyzed by atomic force microscopy using a commercial Nanoscope IIIA Multimode SPM (Veeco instruments, Santa Barbara, C). AFM images were acquired in noncontact tapping mode at scan frequencies of 1−2 Hz under ambient conditions applying a silicon cantilever (NSG01, NT-MDT, Moscow, Russia) with a typical resonance frequency around 150 kHz, a spring constant of 5.5 N/m, and a tip radius below 10 nm. The AFM images, all 512×512 pixels, were quadratic with linear dimensions of 1 and 5.5 μm. The root mean square roughness value as defined in ref 47 as well as the mean length, width, and height of the surface nanostructures was determined by analyzing the AFM images with the Scanning Probe Image Processor (Image Metrology A/S, www.imagemet.com) software. It should be remembered that the finite width of the AFM tip apex may cause a tip convolution, resulting in broadening effects of the surface structure width. The wetting behavior of the surfaces was determined by measuring the contact angle by the sessile drop method, after the substrates were standard treated with UV light/ozone for 25−30 min (Bioforce, Ames, IA) using the contact angle instrument model DSA100 (Krüss, Borssteler Chaussee, Hamburg). Both the Ha and Au coatings were found to be highly hydrophilic after UV treatment with a contact angle below 10°. We used XPS to characterize the surface chemistries of the respective surfaces with a Kratos Axis Ultra^{DLD} instrument equipped with a monochromated Al Kα X-ray source ($h\nu$ = 1486.6 eV) operating at 15 kV and 15 mA (150 W). A hybrid lens mode was employed during analysis (electrostatic and magnetic), with an analysis area of approximately 300 μm × 700 μm. Wide energy survey scans were obtained over the range of 0−1400 eV (corresponding to binding energy) at a pass energy of 160 eV and used to determine the surface elemental composition. The intensity of the individual XPS peaks corresponding to the individual elements present on the surfaces was converted into atomic concentrations with the sensitivity factors proposed by the Vision 2 software package supplied with the Kratos Axis Ultra^{DLD} spectrometer.

Statistical Analysis. Data are expressed as mean ± standard error of mean. Differences between groups were investigated with the two-tailed *t*-test for unpaired samples or the Man-U-Whitney test when the collected data did not follow a Gaussian distribution. Differences were considered significant when $p < 0.05$. The statistical analysis presented in the paper was carried out with Graphpad-Instat 3.0 (GraphPad software, Inc., La Jolla, CA).

Acknowledgment. We gratefully acknowledge the financial support from the Danish Research Councils to the Centre for NeuroEngineering (CNE) and from the Interdisciplinary Nanoscience Center (iNANO).

REFERENCES AND NOTES

1. Kasemo, B. Biological surface science. *Surf. Sci.* **2002**, *500*, 656–677.
2. Stevens, M. M.; George, J. H. Exploring and engineering the cell surface interface. *Science* **2005**, *310*, 1135–1138.
3. Zizak, I.; Paris, O.; Roschger, P.; Bernstorff, S.; Amenitsch, H.; Klaushofer, K.; *et al.* Investigation of bone and cartilage by synchrotron scanning-SAXS and -WAXD with micrometer spatial resolution. *J. Appl. Cryst.* **2000**, *33*, 820–823.
4. Curtis, A.; Wilkinson, C. Nantotechniques and approaches in biotechnology. *Trends. Biotechnol.* **2001**, *19*, 97–101.
5. Kriparamanan, R.; Aswath, P.; Zhou, A.; Tang, L.; Nguyen, K. T. Nanotopography: cellular responses to nanostructured materials. *J. Nanosci. Nanotechnol.* **2006**, *6*, 1905–1919.
6. Flemming, R. G.; Murphy, C. J.; Abrams, G. A.; Goodman, S. L.; Nealey, P. F. Effect of synthetic micro- and nanostructured surfaces on cell behavior. *Biomaterials* **1999**, *20*, 573–588.
7. Curtis, A. S. G.; Varde, M. Control of cell behaviour: Topological factors. *J. Natl. Cancer Inst.* **1964**, *33*, 15–26.
8. Dalby, M. J.; McCloy, D.; Robertson, M.; Wilkinson, C. D. W.; Oreffo, R. O. C. Osteoprogenitor response to defined topographies with nanoscale depths. *Biomaterials* **2006**, *27*, 1306–1315.
9. Peng, L.; Eltgroth, M. L.; LaTempa, T. J.; Grimes, C. A.; Desai, T. A. The effect of TiO_2 nanotubes on endothelial function and smooth muscle proliferation. *Biomaterials* **2009**, *30*, 1268–1272.
10. Rebollar, E.; Frischauf, I.; Olbrich, M.; Peterbauer, T.; Hering, S.; Preiner, J.; *et al.* Proliferation of aligned mammalian cells on laser-nanostructured polystyrene. *Biomaterials* **2008**, *29*, 1796–1806.
11. Dunn, G. A.; Heath, J. P. A new hypothesis of contact guidance in tissue cells. *Exp. Cell. Res.* **1976**, *101*, 1–14.
12. Wilkinson, P. C.; Lackie, J. M. The Influence of contact guidance on chemotaxis of human neutrophil leukocytes. *Exp. Cell. Res.* **1983**, *145*, 255–264.
13. Wan, Y.; Wang, Y.; Liu, Z.; Qu, X.; Han, B.; Bei, J.; *et al.* Adhesion and proliferation of OCT-1 osteoblast-like cells on micro- nanoscale topography structured poly(L-lactide). *Biomaterials* **2005**, *26*, 4453–4459.
14. Zinger, O.; Anselme, K.; Denzer, A.; Habersetzer, P.; Wieland, M.; Jeanfils, J.; *et al.* Time-dependent morphology and adhesion of osteoblastic cells on titanium model surfaces featuring scale-resolved topography. *Biomaterials* **2004**, *25*, 2695–2711.
15. Lovmand, J.; Justesen, J.; Foss, M.; Lauridsen, R. H.; Lovmand, M.; Modin, C.; *et al.* The use of combinatorial topographical libraries for the screening of enhanced osteogenic expression and mineralization. *Biomaterials* **2009**, *30*, 2015–2022.
16. Turner, S.; Kam, L.; Isaacson, M.; Craighead, H. G.; Shain, W.; Turner, J. Cell attachment on silicon nanostructures. *J. Vac. Sci. Technol., B* **1997**, *15*, 2848–2854.
17. Dalby, M. J.; Gadegaard, N.; Tare, R.; Andar, A.; Riehle, M. O.; Herzyk, P.; *et al.* The control of human mesenchymal cell differentiation using nanoscale symmetry and disorder. *Nat. Mater.* **2007**, *6*, 997–1003.
18. Dalby, M. J.; Riehle, M. O.; Sutherland, D. S.; Agheli, H.; Curtis, A. S. G. Fibroblast response to controlled nanoenvironment produced by colloidal lithography. *J. Biomed. Mater. Res* **2005**, *69A*, 314–320.
19. Rice, J. M.; Hunt, J. A.; Gallagher, J. A.; Hanarp, P.; Sutherland, D. S.; Gold, J. Quantitative assessment of the response of primary derived human osteoblasts and macrophages to a range of nanotopography surfaces in a single culture model *in vitro*. *Biomaterials* **2003**, *24*, 4799–4818.
20. Dalby, M. J.; Berry, C. C.; Riehle, M. O.; Sutherland, D. S.; Agheli, H.; Curtis, A. S. G. Attempted endocytosis of nanoenviroment produced by colloidal lithography by human fibroblasts. *Exp. Cell. Res.* **2004**, *295*, 387–394.

21. Dalby, M. J.; Riehle, M. O.; Sutherland, D. S.; Agheli, H.; Curtis, A. S. G. Morphology and microarray analysis of human fibroblasts cultured on nanocolumns produced by colloidal lithography. *Eur. Cell. Mater.* **2005**, *9*, 1–8.
22. Dalby, M. J.; Riehle, M. O.; Sutherland, D. S.; Agheli, H.; Curtis, A. S. G. Changes in fibroblast morphology in response to nano-columns produced by colloidal lithography. *Biomaterials* **2004**, *25*, 5415–5422.
23. Dalby, M. J.; Yarwood, S. J.; Riehle, M. O.; Johnstone, H. J. H.; Affrossman, S.; Curtis, A. S. G. Increasing fibroblast response to materials using nanotopography: morphological and genetic measurements of cell response to 13-nm-High polymer demixed islands. *Exp. Cell. Res.* **2002**, *276*, 1–9.
24. Dalby, M. J.; Childs, S.; Riehle, M. O.; Johnstone, H. J. H.; Affrossman, S.; Curtis, A. S. G. Fibroblast reaction to island topography: changes in cytoskeleton and morphology with time. *Biomaterials* **2003**, *24*, 927–935.
25. Pennisi, C. P.; Sevcencu, C.; Dolatshahi-Pirouz, A.; Foss, M.; Hansen, J. L.; Larsen, A. N.; Zachar, V.; Besenbacher, F.; Yoshida, K. Responses of fibroblasts and glial cells to nanostructured platinum surfaces. *Nanotechnology* **2009**, *20*, 385103.
26. Berry, C. C.; Dalby, M. J.; McCloy, D.; Affrossman, S. The fibroblast response to tubes exhibiting internal topography. *Biomaterial* **2005**, *26*, 4985–4992.
27. Choi, C. H.; Hagvall, S. H.; Wu, B. M.; Dunn, J. C. Y.; Beygui, R. E.; Kim, C. J. Cell interaction with three-dimensional sharp-tip nanotopography. *Biomaterials* **2007**, *28*, 1672–1679.
28. Buttiglieri, S.; Pasqui, D.; Migliori, M.; Johnstone, H.; Affrossman, S.; Sereni, L.; *et al.* Endothelization and adherence of leucocytes to nanostructured surfaces. *Biomaterials* **2003**, *24*, 2731–2738.
29. Riedel, M.; Müller, B.; Wintermantel, E. Protein adsorption and monocyte activation on germanium nanopyramids. *Biomaterials* **2001**, *22*, 2307–2316.
30. Dolatshahi-Pirouz, A.; Pennisi, C. P.; Skeldal, S.; Foss, M.; Chevallier, J.; Zachar, V.; *et al.* The influence of glancing angle deposited nano-rough platinum surfaces on the adsorption of fibrinogen and the proliferation of primary human fibroblasts. *Nanotechnology* **2009**, *20*, 095101.
31. Dalby, M. J.; Riehle, M. O.; Johnstone, H.; Affrossman, S.; Curtis, A. S. G. Investigating the limits of filopodial sensing: a brief report using SEM to image the interaction between 10 nm high nano-topography and fibroblast filopodia. *Cell. Biol. Int.* **2004**, *28*, 229–236.
32. Washburn, N. R.; Yamada, K. M.; Simon, C. G.; Kennedy, S. B.; Amis, E. J. High-throughout investigation of osteoblast response to polymer crystallinity: influence of nanometer-scale roughness on proliferation. *Biomaterials* **2004**, *25*, 1215–1214.
33. Miller, T.; Boettiger, D. Control of intracellular signaling by modulation of fibronectin conformation at the cell-materials interface. *Langmuir* **2003**, *19*, 1723–1729.
34. Dolatshahi-Pirouz, A.; Jensen, T.; Foss, M.; Chevallier, J.; Besenbacher, F. Enhanced surface activation of fibronectin upon adsorption on hydroxyapatite. *Langmuir* **2009**, *25*, 2971–2978.
35. Lan, M. A.; Gersbach, C. A.; Michael, K. E.; Keselowsky, B. G.; Garcia, A. J. Myoblast proliferation and differentiation on fibronectin-coated self assembled monolayers presenting different surface chemistries. *Biomaterials* **2005**, *26*, 4523–4531.
36. Calonder, C.; Matthew, H. W. T.; Van Tassel, P. R. Adsorbed layers of oriented fibronectin: a strategy to control cell-surface interactions. *J. Biomed. Mater. Res.* **2005**, *75A*, 316–323.
37. Michael, K. E.; Vernekar, V. N.; Keselowsky, B. G.; Meredith, J. C.; Latour, R. A.; Garcia, A. J. Adsorption-induced conformational changes in fibronectin due to interactions with well-defined surface chemistries. *Langmuir* **2003**, *19*, 8033–8040.
38. Garcia, A. J.; Ducheyne, P.; Boettiger, D. Effect of surface reaction stage on fibronectin-mediated adhesion of osteoblast-like cells to bioactive glass. *J. Biomed. Mater. Res.* **1998**, *40*, 48–56.
39. Koblinski, J. E.; Wu, M.; Demeler, B.; Jacob, K.; Kleinman, H. K. Matrix cell adhesion activation by non-adhesion proteins. *J. Cell. Sci.* **2005**, *118*, 2965–2974.
40. Barbucci, R.; Magnani, A.; Chiumiento, A.; Pasqui, D.; Cangioli, I.; Lamponi, S. Fibroblast cell behavior on bound and adsorbed fibronectin onto hyaluronan and sulfated hyaluronan substrates. *Biomacromolecules* **2005**, *6*, 638–645.
41. Lord, M. S.; Cousins, B. G.; Doherty, P. J.; Whitelock, J. M.; Simmons, A.; Williams, R. L.; *et al.* The effect of silica nanoparticulate coatings on serum protein adsorption and cellular reponse. *Biomaterials* **2006**, *27*, 4856–4862.
42. Medeiros-Ribeiro, G.; Bratkovski, A. M.; Kamins, T. I.; Ohlberg, D. A. A.; Williams, R. S. Shape transition of germanium nanocrystals on a silicon (001) surface from pyramids to domes. *Science* **1998**, *279*, 353–355.
43. Mo, Y. W.; Savage, D. E.; Schwartzentruber, B. S.; Lagally, M. G. Kinetic pathway in Stranski−Krastanov growth of Ge on Si(001). *Phys. Rev. Lett.* **1990**, *65*, 1020–1023.
44. Müller, B. Natural formation of nanostructures from fundamentals in metal heteroepitaxy to applications in optics and biomaterials science. *Surf. Rev. Lett* **2001**, *8*, 169–228.
45. Müller, B.; Riedel, M.; Michel, R.; De Paul, S. M.; Hofer, R. Impact of nanometer-scale roughness on contact-angle hysteresis and globulin adsorption. *J. Vac. Sci. Technol., B* **2001**, *19*, 1715–1720.
46. Stiehler, M.; Lind, M.; Mygind, T.; Baatrup, A.; Dolatshahi-Pirouz, A.; Li, H.; *et al.* Morphology, proliferation, and osteogenic differentiation of mesenchymal stem cells cultured on titanium, tantalum, and chromium surfaces. *J. Biomed. Mater. Res.* **2008**, *86A*, 448–458.
47. Dolatshahi-Pirouz, A.; Hovgaard, M. B.; Rechendorff, K.; Chevallier, J.; Foss, M.; Besenbacher, F. Scaling behaviour of the surface roughness of platinum films grown by oblique angle deposition. *Phys. Rev. B* **2008**, *77*, 115427.
48. Underwood, P. A.; Steele, J. G.; Dalton, B. A. Effects of polystyrene surface chemistry on the biological activity of solid phase fibronectin and victronectin, analysed with monoclonal antibodies. *J. Cell. Sci.* **1993**, *104*, 793–803.
49. Höök, F.; Kasemo, B.; Nylander, T.; Fant, C.; Sott, K.; Elwing, H. Variations in coupled water, viscoelastic properties, and film thickness of a Mefp-1 protein film during adsorption and cross-linking: a quartz crystal microbalance with dissipation monitoring, ellipsometry, and surface plasmon resonance study. *Anal. Chem.* **2001**, *73*, 5796–5804.
50. Hök, F.; Vörös, J.; Rohdahl, M.; Kurrat, R.; Böni, P.; Ramsden, J. J.; *et al.* A comparative study of protein adsorption on titanium oxide surfaces using *in situ* ellipsometry, optical waveguide lightmode spectroscopy, and quartz crystal microbalance/dissipation. *Colloids Surf., B* **2002**, *24*, 155–170.
51. De Feijter, J. A.; Benjamins, J.; Veer, F. A. Ellipsometry as a tool to study adsorption behavior of synthetic and biopolymers at the air−water interface. *Biopolymers* **1978**, *17*, 1759–1772.
52. Dolatshahi-Pirouz, A.; Skeldal, S.; Hovgaard, M. B.; Jensen, T.; Foss, M.; Chevallier, J.; Besenbacher, F. Influence of Nanoroughness and Detailed Surface Morphology on Structural Properties and Water-Coupling Capabilities of Surface-Bound Fibrinogen Films. *J. Phys. Chem C.* **2009**, *113*, 4406.
53. Dolatshahi-Pirouz, A.; Rechendorff, K.; Hovgaard, M. B.; Foss, M.; Chevallier, J.; Besenbacher, F. Bovine serum albumin adsorption on nano-rough platinum surfaces studied by QCM-D. *Colloids Surf., B* **2008**, *66*, 53–59.
54. Hovgaard, M. B.; Rechendorff, K.; Chevallier, J.; Foss, M.; Besenbacher, F. Fibronectin adsorption on tantalum: the influence of nanoroughness. *J. Phys. Chem. B* **2008**, *112*, 8241–8249.
55. Burridge, K.; Chrzanowska-Wodnicka, M. Focal adhesions, contractility, and signalling. *Annu. Rev. Cell. Dev. Biol.* **1996**, *12*, 463–519.

56. Yamada, K. M.; Geiger, B. Molecular interactions in cell adhesion complexes. *Curr. Opin. Cell. Biol.* **1997**, *9*, 76–85.
57. Hynes, R. O. Cell adhesion: old and new questions. *Trends. Genet.* **1999**, *15*, M33–M37.
58. Aplin, A. E.; Howe, A. K.; Juliano, R. L. Cell adhesion molecules, signal transduction and cell growth. *Curr. Opin. Cell. Biol.* **1999**, *11*, 737–743.
59. Ruoslahti, E.; Ö; brink, B. Common principles in cell adhesion. *Exp. Cell. Res.* **1996**, *227*, 1–11.
60. Galbraith, C. G.; Sheetz, M. P. Forces on adhesive contacts affect cell function. *Curr. Opin. Cell. Biol.* **1998**, *10*, 566–571.
61. Gustafson, T.; Wolbert, L. Studies on the cellular basis of morphogenesis in the sea urchin embryo. *Exp. Cell. Res.* **1961**, *24*, 64–79.
62. Medeiros-Ribeiro, G.; Kamins, T. I.; Ohlberg, D. A. A.; Williams, R. S. Annealing of Ge nanocrystals on Si(001) at 550 °C: metastability of huts and the stability of pyramids and domes. *Phys. Rev. B* **1998**, *58*, 3533–3536.
63. Ross, F. M.; Tromp, R. M.; Reuter, M. C. Transition states between pyramids and domes during Ge/Si island growth. *Science* **1999**, *286*, 1931–1933.
64. Teichert, C.; Lagally, M. G.; Peticolas, L. J.; Bean, J. C.; Tersoff, J. Stress-induced self-organization of nanoscale structures in Si/Ge/Si multilayer films. *Phys. Rev. B* **1996**, *53*, 16334–16337.